Fe@CNT-monoliths for the conversion of carbon dioxide to hydrocarbons: Structural characterisation and Fischer-Tropsch reactivity investigations

Daniel R. Minett,[a] Justin P. O'Byrne,[b] Sofia I. Pascu,[c] Pawel K. Plucinski,[b] Rhodri E. Owen,[c] Matthew D. Jones*[c] and Davide Mattia,*[b]

The direct conversion of carbon dioxide to hydrocarbons with a high economic value, such as olefins, can contribute to preventing further green house gas emissions in the atmosphere. In this paper, we report a synthesis, characterisation and catalytic study centred onto iron nanoparticle-carbon nanotube arrays grown on monoliths (Fe@CNT-m). These have been used for the catalytic conversion of carbon dioxide to hydrocarbons, showing superior properties than the powder form. The monolith-supported structure also overcomes limitations of the powder catalyst, such as high-pressure drops and potential toxicity of airborne CNT powders, that have, so-far, limited its use in industry. The optimal process conditions (temperature pressure, flow rate and reaction time) have been identified along with deactivation mechanisms. The different catalytic performance of the residual iron NPs outside and inside the CNTs has also been investigated.

1. Introduction

The utilisation of carbon dioxide as a feedstock for long chain olefin production has been the holy grail for the chemical community over the past decades,[1] as its availability could represent a way to mitigate the effects of climate change.[2] One widely explored method is to combine the reverse water gas shift (RWGS) process with the Fischer-Tropsch (FT) process to produce hydrocarbons using carbon dioxide as a feedstock.[3] The combination of the two reactions is thermodynamically viable,[4] but requires the use of catalysts capable of facilitating both processes.[5-7] Typical approaches have involved using iron-based FT catalysts that are known to catalyse both reactions, *via* the formation of oxides and carbides with different activities.[8, 9 7] Compared to other commonly used FT catalysts, such as cobalt,[6] iron gives the best selectivity towards higher order hydrocarbons and away from methane - the most stable thermodynamic product.[2, 3, 10] The latter is key to the commercial success of this technology, particularly now with the low prices for so-called "shale-gas".

We recently demonstrated that residual iron nanoparticles (NPs) from the carbon nanotube synthesis process can be activated in-line and the resulting Fe@CNT supports are active for both the RWGS reaction and the FT process to yield hydrocarbons, using CO_2 as the feedstock.[11] Hereby, carbon nanotubes are acting as catalytic supports of choice due to their high surface area, thermal stability and good adhesion to metal particles.[12-14] CNTs have been used extensively as supports for the conversion of carbon monoxide to hydrocarbons, with a higher activity per unit volume than other supports due to superior catalyst dispersion,[15] as well as affording higher selectivity to olefins.[16] Iron nanoparticles deposited onto CNTs *via* incipient wetness methods have shown to be effective FT catalysts,[17] with low deactivation rates.[18] Iron supported on carbon nanofibres (CNF) has been shown to provide high selectivity to short olefins using CO as feedstock.[19] Furthermore, differences in conversion and selectivity has been observed for iron nanoparticles on the outside surface and in the bore of carbon nanotubes.[20] On the other hand, carbon nanotubes in powder form have a number of disadvantages for industrial applications, including a high-pressure drop for gas phase processes, and agglomeration. Coupled with health and safety concerns related to large-scale airborne presence of CNTs, these aspects have, so far, limited the applicability of such catalysts in industrial settings. To mitigate some of these limitations a number of groups have recently endeavoured to prepare bulk nanotube catalysts by growing CNT on structured supports.[20-22] We have previously developed a method for growing CNTs directly onto a structured cordierite monoliths without wash-coating or other pre-treatment steps.[23] The uniform coatings of CNTs produced in this manner have low pressure drop and high mechanical stability, thereby addressing the main drawbacks of CNTs as catalyst supports.

In this paper, we report the synthesis, characterisation and catalytic study of iron nanoparticle-carbon nanotube arrays grown on monoliths (Fe@CNT-m). These have been used for the catalytic conversion of carbon dioxide to hydrocarbons, showing superior properties than the powder form. The different catalytic performance of the residual iron NPs outside and inside the CNTs has also been investigated and is discussed herein.

2. Experimental

Catalyst synthesis procedure

Aligned arrays of CNTs were grown on multiple pieces of 0.9 cm diameter × 1 cm long cordierite monoliths *via* an aerosol based chemical vapour deposition (CVD) of ferrocene (0.2 g) dissolved in toluene (10 ml).[23] The ferrocene–toluene solution was injected using a syringe pump at a rate of 10 ml h^{-1} under 450 sccm Ar and 50 sccm H_2 into a quartz tube at 790 °C for 60 minutes. The resulting layer is 80-100 µm thick, and makes up ~5% by weight of the resulting monolith composite (Fig. 1). The thickness of the CNT arrays can be controlled by varying the CVD time.

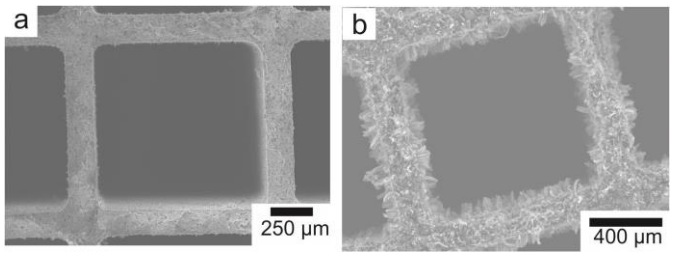

Fig. 1 SEM micrographs of a) bare cordierite monolith and b) cordierite monolith coated with CNT layer

The resulting tubes had residual iron NPs on the outer surface (Fig.2a) as well as enclosed within the core of the CNT (Fig. 2c). The iron NPs on the external surface are coated with a graphitic layer (Fig.2b), which renders them inactive for the hydrogenation of CO_2.[11]

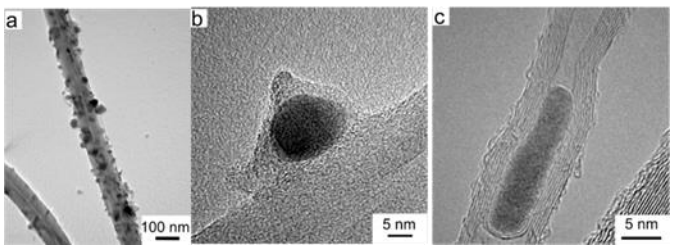

Fig. 2 TEM micrographs of as-produced CNTs showing the presence of Fe nanoparticles a) on the surface and, at higher magnification, b) a Fe nanoparticle covered with a graphitic layer or c) confined within the CNT bore

Activation of the iron nanoparticle-CNTs (i.e. removal of the graphitic layers coating the Fe NPs) on the monolith was initially attempted replicating the same conditions used for the powder (570 °C in air for 30 minutes). Whereas the graphitic CNTs were unaffected in powder form by this process, the CNTs on the monolith, produced with the same synthesis condition showed complete degradation, probably due to the thermal inertia of the cordierite support. Reducing the temperature (470 °C) and time (10 minutes) of oxidation was sufficient to activate the NP on the monolith without degrading the CNTs.

Catalytic testing

To test the catalytic activity, 10 monoliths (0.9 mm diameter ×1 cm length) were loaded into a purpose built stainless steel reactor (½″ diameter × 10 cm length). The catalyst was reduced under a flow of 50 sccm of hydrogen for 2 hours at 370 °C. Subsequently, the feed mixture was changed to 8 sccm CO_2/H_2 in 1:3 ratio. Each test was run for 6 hours at 370 °C, with gas samples analysed every hour. The product gases were analysed using GC-MS following our previously reported optimised method.[11] In all cases, the mass balance was found to be satisfactory and within the range of experimental error. The Anderson-Schulz-Flory model (e.g. typically used to predict the product distribution)[5] indicates that the maximum selectivity for the C_2-C_4 fraction occurs at a chain growth probability (α) of between 0.4 and 0.5.[19] Calculated values of α for these catalysts fall in or around this optimum range. The observed rate of reaction was estimated by dividing the number of moles of CO_2 converted per second, by the total mass of CNT present in the reactor. FTY, iron time yield, was determined by dividing the number of moles of CO_2 converted per second by the mass of iron present in the catalyst. FTY has been determined using the amount of surface iron present (as determined by XPS and EDX), and the total amount of iron present in the catalyst (as determined by TGA analysis).

Nano-Catalyst Characterisation

TEM imaging was carried out on a JEOL 1200 operated at 120 kV; HRTEM imaging was carried out on a JEOL 2100 (LaB6 filament) instrument operated at 200 kV. Samples for TEM analysis were scraped from the monolith, dispersed in ethanol and deposited onto Cu or Ni grids. SEM was carried out on a JEOL 6480LV at 5–25 kV. Raman spectra were recorded between 100 and 3000 cm^{-1} using a Renishaw Invia spectrometer, using a 532 nm laser, with laser power set to 5%, to avoid burning the tubes. Powder X-ray diffraction (pXRD) patterns were recorded with Co $K\alpha_{1,2}$ radiation from 20 to 90 degrees (2θ), typically at a scan rate of 1.34 degrees/min, at ambient temperature using a Panalytical X'Pert Pro X-ray diffractometer. Experiments were performed in flat-plate mode. *In situ* pXRD experiments were carried out using an Anton Paar XRK900 reaction chamber under flow conditions. Experiments were performed in flat-plate mode. Typically, the scan range was 25 to 65 degrees (2θ), and at a scan-rate of 1.34 degrees/min. The system was flushed with helium, at a flow of 30 sccm. Oxidation was carried out under a flow of 30 sccm of air. Reduction was carried out under a flow of 30 sccm of hydrogen. Reactions were performed under 30 sccm H_2 and 10 sccm CO_2. It was not possible to obtain meaningful pXRD of the Fe@CNT powder grown on the monoliths, as this contained residual amounts of cordierite, which dominated the resulting pXRD patterns.

3. Results and Discussion

Catalytic Testing

The Fe@CNT-m were first tested under the same conditions for the powder catalyst:[11] Using a 10 cm long reactor at ambient pressure and 370 °C for 6 hours. The presence of the monolith ensured that for the same reactor volume, the mass of catalyst would be significantly lower than in the powder case (0.15 g *cf.* 0.4 g for the powdered catalyst). This resulted in a conversion of 4.6 % compared to a value of 15.9 % for the powder catalyst, with 97 % selectivity to carbon monoxide and little to no hydrocarbons (Table 1, entry 1).

Table 1. Conversion and selectivity data as a function of reactor pressure

Pressure (bar)	Conversion %	FTY (10^{-5})/mol $g^{-1}s^{-1}$ surf. Fe	FTY (10^{-5})/mol $g^{-1}s^{-1}$ all Fe	FTY (10^{-5})/mol $g^{-1}s^{-1}$ CNT+Fe	Selectivity/% CO	C_1	C_{2-4}	C_{5+}	α
1.0	4.6	27.5	0.14	0.04	96.9	2.8	0.3	0	0.19
2.5	9.0	31.8	0.28	0.08	46.6	38.6	14.8	0	0.30
5.0	18.5	30.9	0.57	0.17	64.6	26.2	9.1	0	0.35
7.5	32.2	29.5	0.98	0.30	16.1	47.5	31.8	4.6	0.47
10.0	32.0	17.1	1.03	0.31	17.5	48.7	30.6	3.2	0.44
12.5	34.6	8.39	1.06	0.32	14.4	45.5	35.3	4.7	0.52
15.0	29.6	4.20	0.92	0.28	21.7	49.1	26.8	2.4	0.44

The powder and supported catalyst were also compared at 7.5 bar and 370 °C for 6 hours. The volumetric comparison shows similar conversion but the reaction rate of the supported catalyst is triple that of the powder (Fig. 3, first two set of columns). Comparison on a mass basis was achieved by dispersing 0.15 g of Fe@CNT powder in 0.25 g of un-activated CNTs. In this case, the conversion of the Fe@CNT-m also is roughly three times that of the powder catalyst.

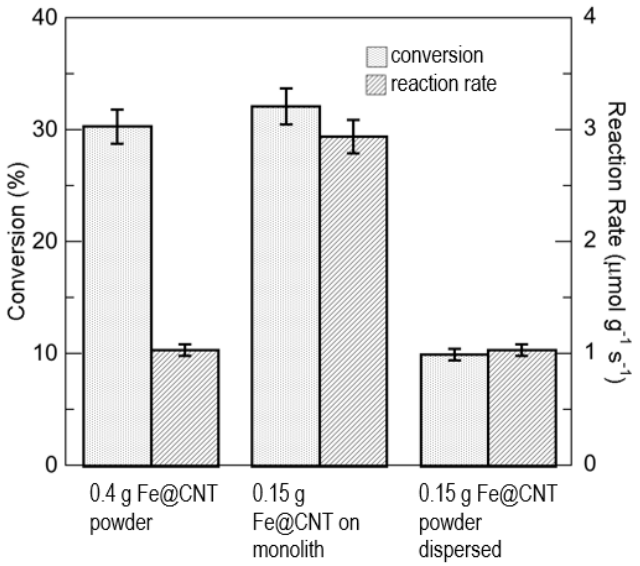

Fig. 3 Volumetric (first two sets of columns) and weight (second set of columns) comparison of the powder and monolith supported Fe@CNT for total conversion and rate of reaction (conditions: 7.5 bar, 370 °C for 6 hours)

Increasing the reaction pressure for the monolithic catalyst showed an increase in conversion until 7.5 bar, after which conversion appears to reach a maximum (Fig. 4), suggesting that at this point the reaction becomes rate limited. This improvement in performance is due to the shifting of the equilibrium of the reaction to higher hydrocarbons with increasing pressure. With increased pressure alpha gradually increases before plateauing at around 0.5. This is not surprising as increased pressure is well known to shift the process towards higher molecular weight products.[24]

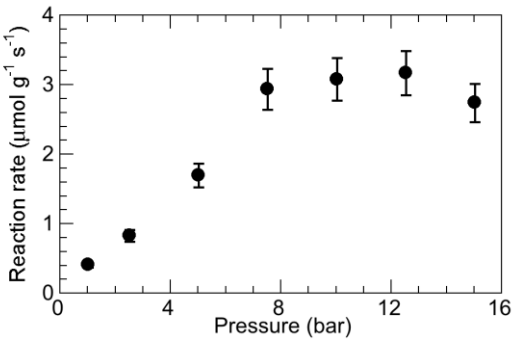

Fig. 4 Effect of pressure variation on rate of CO_2 conversion. The reaction was performed at 370 °C over a 10 cm bed of Fe@CNT/monolith (synthesised at 790 °C for 60 minutes, approximately 0.15 g of Fe@CNT, activated by 10 minutes oxidation at 470 °C). Total flow rate = 8 sccm (CO_2 to H_2 ratio 1:3).

Conversion also increases with temperature up to 370 °C, after which it no longer increases, suggesting that the reaction is no longer rate limited, possibly entering a mass transfer controlled region. The reaction temperature plays an important role in the activity of the catalyst. Figure 5 plots the natural logarithm of total conversion of CO_2 or hydrocarbon yield against the inverse of the temperature. Two different regions can clearly be observed: At temperatures below 350 °C, the reaction temperature is rate controlling and above 350 °C the reaction rate no longer increases, suggesting the rate determining step is presumably the diffusion of the reactants to the surface.

For the reaction-controlled regions, an apparent activation energy for the reactions can be determined. The apparent activation energy for the conversion of CO_2 to CO is 34.9 kJ mol^{-1}, whilst the activation energy for the subsequent conversion to hydrocarbons is 82.8 kJ mol^{-1}. Reported values for the activation energy of the reverse water gas shift reaction vary dramatically with values from 40 to 120 kJ mol^{-1} previously reported for a wide variety of catalysts.[25] [26] The reported value for FT synthesis is within the range of those recently reported for iron catalysts (63-89 kJ mol^{-1}).[26]

The observed rate of reaction (~3 μmol g_{CNT}^{-1} s^{-1}) above 7.5 bar (at 370 °C) is significantly higher than that observed for a Fe/CNF catalyst at 350 °C and 1 bar,[19] or for a 20 wt% Fe/O-CNT catalyst at 340 °C and 20 bar.[27] In both cases CO was the feedstock rather than CO_2. When using carbon dioxide as feedstock, a comparable Fe/Al_2O_3 catalyst had an activity of 0.83 μmol $g^{-1}s^{-1}$ at a higher temperature (400 °C) and higher pressure (20 bar).[28] Potassium doping did not increase the activity beyond 1.23 μmol g_{CNT}^{-1} s^{-1}. The same catalyst had a comparable activity of 0.52 μmol g^{-1} s^{-1} at 300 °C and 10 bar, with a variety of different dopants providing little difference. On the other hand, unsupported Fe/Mn/K nanofibres at 260 °C

and 13.7 bar showed double the activity using a fixed bed reactor.[29] Higher activities at these low temperatures, upwards of 1 μmol g^{-1} s^{-1}, were also observed in a CSTR for a $Fe/Mn/K/Al_2O_3$ catalyst,[30] but the activity dropped by an order of magnitude for the same catalyst in a fixed bed reactor.[31]

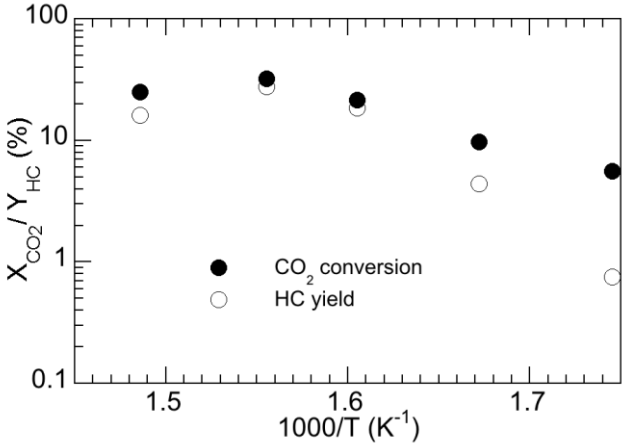

Fig. 5 Effect of temperature variation on CO_2 conversion. The reaction was performed at 7.5 bar over a 10 cm bed of Fe@CNT/monolith (synthesised at 790 °C for 60 minutes, approximately 0.15 g of Fe@CNT), temperature was varied from 300 to 400 °C.

The selectivity of the process does not show a strong dependence on temperature, with alpha values remaining invariant over the temperature range investigated. At 400 °C, however, a significant drop in alpha is observed, as previously observed for a $Fe/Al_2O_3/Cu/K$ catalyst.[26] In that case it was suggested that this drop in selectivity is most likely due to an increase in the rate of the Boudouard reaction (the disproportionation of CO to afford elemental carbon and CO_2).[26] As our support is made of carbon, it is not possible to confirm this mechanism for Fe@CNTs.

Olefin selectivity is higher than that reported for CO_2 reduction using a Fe/Al_2O_3 catalyst (0.06),[28] but significantly lower that what reported for a FT iron catalyst supported on carbon nanofibres (0.94),[19] and a Fe/O-CNT one (0.41).[27] This superior olefin selectivity is due to the presence of trace amounts of K dopant, as well as the effect of a weakly interacting support.

The flow-rate of the gas mixture can be seen to have a significant impact on the conversion of CO_2 over the Fe@CNT-m (Fig. 6). The overall conversion decreases with increasing flow-rate, progressing from conversions as high as 41.9 % at the low overall flow-rate of 4 sccm, to conversions as low as 13.4 % at the higher overall flow-rate of 16 sccm (Fig. 5, inset). The overall conversion, and the conversion to hydrocarbons both decrease linearly with increased flow rates. It can clearly be seen that the reaction has not gone to completion and changing the flow rate dramatically changes the apparent conversion. The majority of literature regarding CO_2 conversion reports results in terms of overall conversion, which is useful for comparison between catalysts using the same system, but the clear influence of flow rate on the overall conversion must be considered when comparing catalysts between different systems.[32] A more informative comparison between systems can be obtained by reporting the observed rate of CO_2 conversion per gram of catalyst per second. This observed rate of reaction cannot be considered to be a true rate of reaction, as with larger values of conversion differences in the change in the reactant mix will affect the rate. In our system the observed reaction rates remain constant as the flow rate is varied implying that the flow rate has little effect on the actual rate of reaction. However, changing the flow rate significantly shifts the observed product distribution. Higher total flows shifting the product distribution towards carbon monoxide. ASF distributions, calculated for each flow rate, showed very little change however, with calculated alpha values consistently being in the range 0.44 - 0.47. The higher flow rates shifting the product distribution would therefore seem to be due to decreasing residence time.

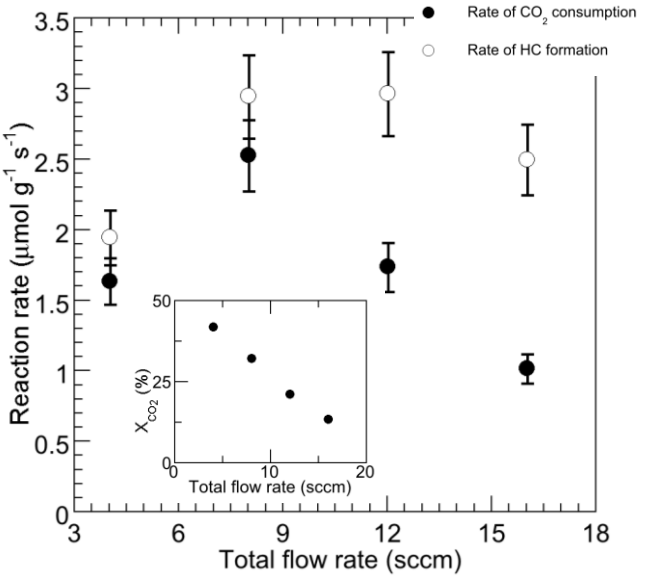

Fig.6 Carbon dioxide consumption and hydrocarbon production as a function of total flow rate. Effect of changing flow rate on CO_2 reaction rate, the reaction was performed at 370 °C over a 10 cm bed of Fe@CNT/monolith (synthesised at 790 °C for 60 minutes, approximately 0.15 g of Fe@CNT, activated by 10 minutes oxidation at 470 °C) at 7.5 bar. Total flow rate was varied from 4-16 sccm using a CO_2 to H_2 ratio of 1:3. The inset shows the CO_2 conversion with total flow rate.

Catalyst Analysis

The oxidation, reduction and reaction process of the Fe@CNT powder were followed by *in-situ* pXRD to determine the nature of the catalytic species formed at each stage. High-resolution TEM micrographs and EDX analysis (Fig. S1) were performed on the catalyst after preparation, oxidation and post-reaction in order to observe changes in the graphitic layer. The *in-situ*

pXRD showed clear changes in the species present on the catalyst at each stage of the reaction (Fig. 7).

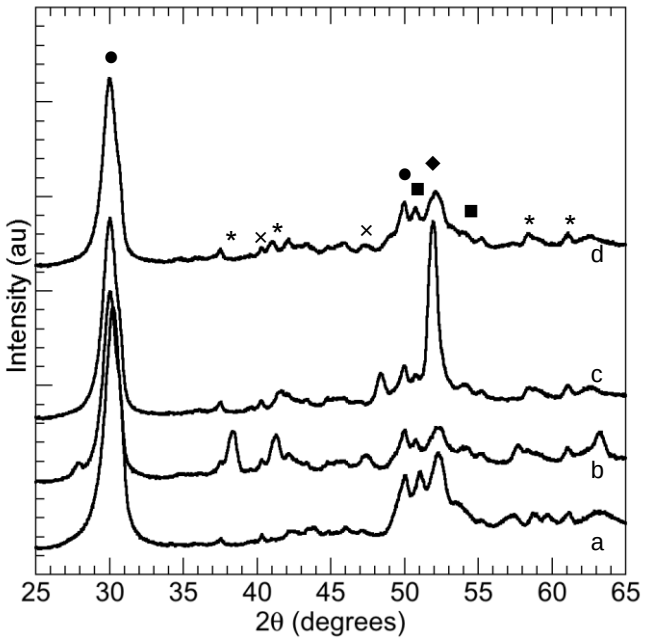

Fig. 7 pXRD spectra of Fe/CNT powder after a) synthesis at 790 °C for 60 minutes b) oxidation at 470 °C c) hydrogenation at 370 °C for 2 hours d) reaction at 370 °C for 4 hours • CNT, * Fe_2O_3 haematite, × Fe_3O_4 magnetite, ■ Fe_3C cementite, ♦ Fe(0) iron metal

After synthesis and before any further treatment the pXRD spectrum (Fig. 7a, as produced) shows peaks corresponding to CNT, metallic iron and an iron carbide species, which is a good match for cementite Fe_3C (*N.B.* this assignation should be treated with some caution as diffraction patterns for iron carbide species can have very similar peak positions). TEM micrographs of CNT after synthesis on the monolith (Fig. 2b and 2c) clearly show the presence of iron in two distinct environments; 1) on the surface of the nanotube, coated with a graphitic layer, and 2) inside the nanotube. EDX analysis cannot determine whether this is purely metallic iron or carbide, due to background carbon signal from the CNT. However, no oxygen was detected confirming the absence of an oxide species (Fig. S1). Previous *in-situ* studies have observed the presence of both metallic iron and Fe_3C in the growth phases of CNTs.[33, 34] These species have also been previously detected after growth.[35]

As previously stated, the graphitic layer prevents access to the iron nanoparticles. Oxidation can remove this graphitic layer, but can also oxidise the nanoparticles formed. This is clearly seen in the XRD pattern (Fig. 7b, post-oxidation). Firstly, two major peaks are immediately observed and are assigned to iron oxide haematite (Fe_2O_3), the most stable form of iron oxide. Also observed are a number of peaks belonging to magnetite (Fe_3O_4), which largely overlap with the minor Fe_2O_3 peak at 42 °. Longer oxidations lead to an increase in the haematite and a corresponding decrease in the iron and cementite peaks centred around 52 °. This is to be expected, suggesting that the iron and cementite are being oxidised to more stable oxide forms such as haematite and magnetite. As the oxidation progresses, the CNT peak at 31 ° also begins to decrease. This is due to the exposed iron oxide nanoparticles beginning to catalyse the decomposition of the CNT. These results do, however, support the experimental finding that oxidation for an extended period can result in decomposition of the CNT. This decomposition begins before all iron particles in the sample are exposed and oxidised, as many are buried deep within the CNT core. As such is it not beneficial to continue the oxidation until all iron nanoparticles are oxidised. Oxidation of cementite is shown to produce both haematite and magnetite,[36] whilst oxidation of pure iron is shown to produce wursite ($Fe_{0.95}O$) and magnetite initially, before forming haematite at high temperatures.[11] The expected pathway of the oxidation of cementite sees the formation of magnetite followed by further oxidation to haematite.[36]

TEM micrographs and EDX analysis clearly show the effects of oxidation of the CNT on the monolith (Fig. 8). Exposed nanoparticles can be observed on the surface of the CNT, at the tips of the now opened nanotubes, and inside the nanotube core.

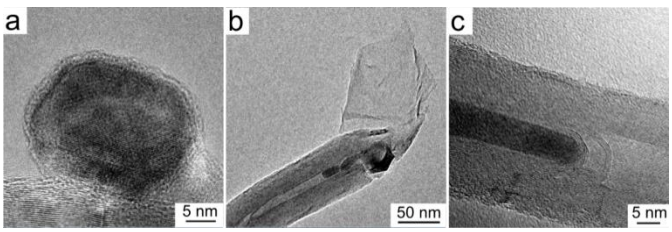

Fig. 8 TEM micrographs of CNT taken from the monolith surface showing a) exposed nanoparticles on the surface of the nanotube b) exposed nanoparticle at the end of the nanotube c) nanoparticles still enclosed by the nanotube

EDX analysis confirms that the iron nanoparticles on the surface of the CNT have been partially oxidised, with a Fe:O ratio of 1:1, compared to the absence of oxygen before oxidation (Fig. S1). The iron nanoparticle at the nanotube tip is less oxidised, suggesting that the iron still enclosed in the nanotube has not been oxidised. Iron detected inside the nanotubes shows the presence of minimal amounts of oxygen, with a Fe:O ratio of 10:1. This suggests that the iron in the inner core remains in its metallic or carbide form.

Hydrogenation causes another change in the iron species detected (Fig 7c, post-hydrogenation). Haematite is very quickly converted into iron metal and a variety of reduced iron oxides, the major species being wursite and magnetite. Longer hydrogenations lead to a slight decrease in the magnetite peak and a slight increase in the iron metal and wursite peaks. The rapid conversion of haematite to iron metal and wursite indicates that hydrogenating the catalyst for longer periods would seem to have little effect on the resulting catalyst, with perhaps the only effect being the reduction of the remaining magnetite to iron metal. As magnetite is a known reverse water gas shift catalyst this may have an adverse effect for this reaction.

The authors have previously reported that *in situ* XPS of the powder catalyst after hydrogenation showed Fe_3O_4 as the main species with little iron metal or carbide detected.[11] Due to the nature of XPS, this can only by ascribed to the nanoparticles on the outer CNT surface. The pXRD shown here, in contrast, analyse the iron both on the surface and in the tubes. This allows us to ascribe the metal iron / iron carbide signal primarily to the iron in the inner core of the CNT. Previous authors have observed that encapsulated nanoparticles can have very different reduction environments compared to those supported on the outside of the CNT.[37] They found that iron NPs confined within the CNT could be reduced relatively easily at temperatures where nanoparticles on the surface of the nanotube remained as iron oxide.[38]

Introduction of CO_2 and H_2 into the reaction chamber again causes a rapid change in the iron phases (Fig 7d, post-reaction). Exposure of the catalyst to the carbon dioxide and hydrogen atmosphere readily leads to the formation of iron carbides.[39] Determination of the carbide species from pXRD can be problematic, due to peak overlap, however it appears to be a mixture of cementite (Fe_3C) and the Hagg carbide (Fe_5C_2), which are both known to be active Fischer-Tropsch catalysts.[39, 40] This process is equally rapid when CO_2 is substituted for CO. It is unclear whether the CO_2 is first converted into CO which then reacts and forms the carbide species, or whether CO_2 itself can form carbide species directly. It is to be noted that after carburisation, no oxide species can be detected *via* pXRD, unlike previous studies performing Fischer-Tropsch synthesis, where iron oxide and iron carbides have been observed to co-exist.[38] This is surprising as the water gas shift reaction is traditionally thought to be catalysed by these oxide species and not by the iron carbide.[41] Previous studies on CNT for the FT process have also demonstrated surprising water gas shift activity despite little iron oxide being detected.[27] This was thought to be due to the presence of amorphous iron oxide that was not picked up by pXRD. *In situ* XPS demonstrated the presence of iron oxide on the surface of the catalyst after reduction. Thus, it is likely that this iron oxide, undetected by pXRD, constitutes the active species for the reverse water gas shift reaction.

Catalyst stability

A concern with the use of carbon catalysts must be that the support itself does not decompose and contribute to the products detected. The stability of the CNTs when exposed to a pure stream of hydrogen and CO_2 was examined. The CNTs were tested as produced and after activation. During hydrogenation, in both cases very small amounts of methane (0.01 %) were detected when placed in a gas stream of 8 sccm hydrogen, though the evolution of methane decreased over the 2 hours tested. The majority of this evolved hydrogen is observed during the hydrogenation step prior to reaction, and hence should not interfere with catalytic data. After hydrogenation the catalyst was placed under a stream of pure carbon dioxide (8 sccm) with no other species detected.

The stability of the CNT-supported catalyst was also estimated using TGA. Apart from a reduction in mass under hydrogen at 340 °C (corresponding to the reduction of iron oxide to metallic iron), the CNTs remain stable at temperatures greater than the reaction temperature, with decomposition of the CNT beginning above 500 °C under hydrogen, and with very little decomposition observed under CO_2, until over 600 °C. The Fe@CNT-m shows distinct de-activation over time with activity decreasing continuously over the 15 hours tested (Fig. 9).

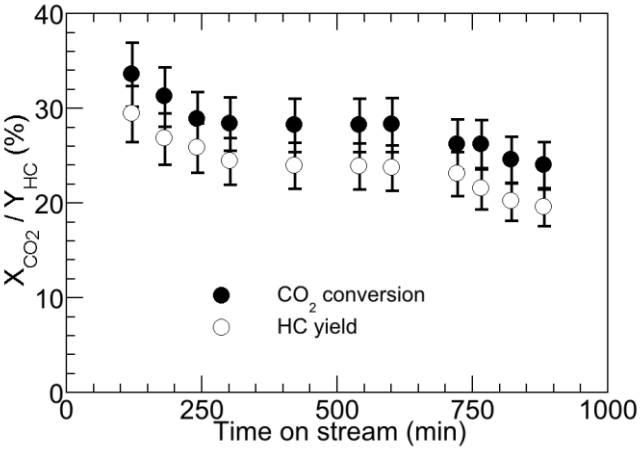

Fig. 9 Effect of time on stream on CO_2 conversion, the reaction was performed at 370 °C over a 10 cm bed of Fe@CNT/monolith (synthesised at 790 °C for 60 minutes, approximately 0.15 g of Fe@CNT, activated by 10 minutes oxidation), at 7.5 bar. Total flow rate = 8 sccm (CO_2 to H_2 ratio 1:3).

Time on-stream refers to the total time under reaction conditions. The change in performance over time is not insignificant, with approximately 30% of the total activity lost over the 15 hours on-stream. The origins of the deactivation mechanism observed here are not well understood. A number of deactivation mechanisms can occur in Fischer-Tropsch synthesis including poisoning, sintering, phase changes or carbon deposition.[5] Poisoning is usually the result of the presence of sulphur in the feed;[5] as no sulphur is present in this case this can most likely be ruled out as a potential cause. Deactivation due to phase changes of the active species to less active species is possible, however observation of the catalyst via *in-situ* pXRD shows no change over the two hours monitored. Since deactivation occurs continuously from the start of the reaction, it would be expected to see some change in the phase of the active species. This leaves sintering or carbon deposition as the two most probable causes of deactivation, or more likely a mix of the two. Carbon deposition is difficult to determine on a carbon-based catalyst, as the presence of the carbon catalyst masks deposited carbon from most detection methods. Deposition of amorphous carbon on the nanoparticle surface was not observed *via* high resolution TEM. Re-oxidation and re-hydrogenation, or simply re-hydrogenation did not recover the catalytic activity. After reaction TEM micrograph show the presence of agglomerations of larger iron nanoparticles on the surface of the CNT (Fig. 10), not observed

for the as-prepared nanotubes, or after oxidation. There is some evidence in the literature that upon prolonged exposure to reaction conditions the nanoparticles on the surface of the tube can migrate forming nanoparticle clusters on the surface of the tube.[5, 42]

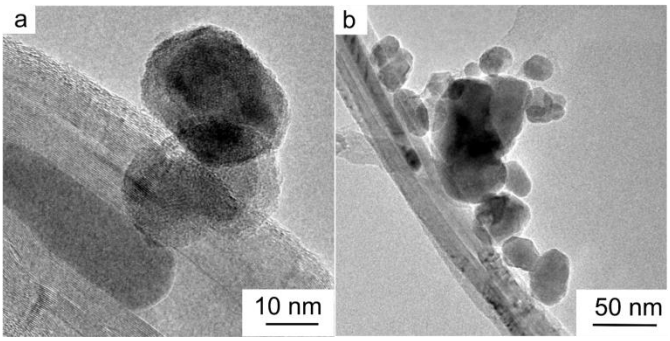

Fig. 10 TEM micrographs (a) and (b) showing agglomerations of iron nanoparticles observed by TEM after the reaction completion.

4. Conclusions

This work has demonstrated that CNTs grown on the surface of cordierite monoliths can be activated in a similar manner to powdered CNTs, by removal of the graphitic layer surrounding residual iron nanoparticles *via* a controlled oxidation. The resulting substrate has a poorer performance to the powder catalyst at atmospheric pressure, but can achieve similar conversions and a higher rate of reaction at high pressure. Experimental evidence suggests that when pressure is increased beyond 7.5 bar, the reaction is mass-transfer limited, rather than rate-limited.

Detailed studies of the catalyst *via* HR-TEM, EDX and pXRD have revealed that the iron nanoparticles present in the catalyst vary significantly throughout the process. The formation of iron carbides, which are believed to catalyse the FT process, is to be expected but it is surprising that iron oxide species are not detected *via* pXRD. XPS measurements suggest that magnetite species are present on the CNT surface, but these are not detected by pXRD. The presence of magnetite on the surface of the nanotube, and iron carbides in the catalyst bore may explain the effectiveness of the CNT catalyst for CO_2 conversion.

Acknowledgements

The authors wish to acknowledge Dr Zabeada Aslam (LENFF) for electron microscopy and XPS/XRD analysis, the ESPRC (grant EP/H046305/1), and the University of Bath for funding. We are extremely grateful to Dr. Philip Landon (SASOL Technology) for experimental assistance with the pXRD measurements. DRM acknowledges funding from the CDT in Sustainable Chemical Technologies at the University of Bath. SIP is supported by a RS URF.

5. Notes and references

[a] *Doctoral Training Centre in Sustainable Chemical Technologies, University of Bath, Bath BA2 7AY, UK*

[b] *Department of Chemical Engineering, University of Bath, Claverton Down,Bath BA2 7AY, UK E-mail d.mattia@bath.ac.uk*

[c] *Department of Chemistry, University of Bath, Claverton Down, Bath BA2 7AY, UK.E-mail mj205@bath.ac.uk*

Electronic Supplementary Information (ESI) available: [details of any supplementary information available should be included here]. See DOI: 10.1039/b000000x/

1. M. Aresta and A. Dibenedetto, *Dalton Trans.*, 2007,, 2975-2992.
2. G. Centi, E. A. Quadrelli and S. Perathoner, *Energy & Environmental Science*, 2013, 6, 1711-1731.
3. R. W. Dorner, D. R. Hardy, F. W. Williams and H. D. Willauer, *Energy & Environmental Science*, 2010, 3, 884-890.
4. L. Torrente-Murciano, D. Mattia, M. D. Jones and P. K. Plucinski, *Journal of CO2 Utilization*, 2014, 6, 34-39.
5. E. de Smit and B. M. Weckhuysen, *Chem. Soc. Rev.*, 2008, 37, 2758-2781.
6. R. E. Owen, J. P. O'Byrne, D. Mattia, P. Plucinski, S. I. Pascu and M. D. Jones, *Chem. Commun.*, 2013, 49, 11683-11685.
7. R. E. Owen, J. P. O'Byrne, D. Mattia, P. Plucinski, S. I. Pascu and M. D. Jones, *ChemPlusChem*, 2013, 78, 1536-1544.
8. M. E. Dry, *Catal. Today*, 2002, 71, 227-241.
9. E. S. Lox and G. F. Froment, *Ind Eng Chem Res*, 1993, 32, 71-82.
10. W. Wang, S. P. Wang, X. B. Ma and J. L. Gong, *Chem. Soc. Rev.*, 2011, 40, 3703-3727.
11. J. P. O'Byrne, R. E. Owen, D. R. Minett, S. I. Pascu, P. Plucinski, M. D. Jones and D. Mattia, *Catal. Sci. Technol.*, 2013, 3, 1202-1207.
12. Y. A. Kim, H. Muramatsu, T. Hayashi, M. Endo, M. Terrones and M. S. Dresselhaus, *Chem. Phys. Lett.*, 2004, 398, 87-92.
13. F. Rodríguez-reinoso, *Carbon*, 1998, 36, 159-175.
14. G. G. Wildgoose, C. E. Banks and R. G. Compton, *Small*, 2006, 2, 182-193.
15. B. Sun, K. Xu, L. Nguyen, M. H. Qiao and F. Tao, *ChemCatchem*, 2012, 4, 1498-1511.
16. E. van Steen and F. F. Prinsloo, *Catal. Today*, 2002, 71, 327-334.
17. M. C. Bahome, L. L. Jewell, D. Hildebrandt, D. Glasser and N. J. Coville, *Appl. Catal. A-Gen.*, 2005, 287, 60-67.
18. R. M. M. Abbaslou, A. Tavasoli and A. K. Dalai, *Appl. Catal. A-Gen.*, 2009, 355, 33-41.
19. H. M. Torres Galvis, J. H. Bitter, C. B. Khare, M. Ruitenbeek, A. I. Dugulan and K. P. de Jong, *Science*, 2012, 335, 835-838.
20. P. Serp and E. Castillejos, *ChemCatChem*, 2010, 2, 41-47.
21. N. A. Jarrah, J. G. van Ommen and L. Lefferts, *J. Mater. Chem.*, 2004, 14, 1590-1597.
22. E. García-Bordejé, I. Kvande, D. Chen and M. Rønning, *Adv. Mat.*, 2006, 18, 1589-1592.
23. D. R. Minett, J. P. O'Byrne, M. D. Jones, V. P. Ting, T. J. Mays and D. Mattia, *Carbon*, 2013, 51, 327-334.
24. M. E. Dry, *Catal. Today*, 2002, 71, 227-241.
25. R. Smith, L. Muruganandam and S. S. Murthy, *ChemInform*, 2010, 41.
26. T. Riedel, G. Schaub, K.-W. Jun and K.-W. Lee, *Ind Eng Chem Res*, 2001, 40, 1355-1363.
27. H. J. Schulte, B. Graf, W. Xia and M. Muhler, *ChemCatChem*, 2012, 4, 350-355.
28. P. S. Sai Prasad, J. Bae, K.-W. Jun and K.-W. Lee, *Catal Surv Asia*, 2008, 12, 170-183.
29. B. Hu, S. Frueh, H. F. Garces, L. Zhang, M. Aindow, C. Brooks, E. Kreidler and S. L. Suib, *App Catal B: Env*, 2013, 132–133, 54-61.
30. R. W. Dorner, D. R. Hardy, F. W. Williams and H. D. Willauer, *App Catal A: General*, 2010, 373, 112-121.

31. D. M. Drab, H. D. Willauer, M. T. Olsen, R. Ananth, G. W. Mushrush, J. W. Baldwin, D. R. Hardy and F. W. Williams, *Energy Fuels*, 2013, 27, 6348-6354.
32. G. Centi, G. Iaquaniello and S. Perathoner, *ChemSusChem*, 2011, 4, 1265-1273.
33. M. J. Behr, E. A. Gaulding, K. A. Mkhoyan and E. S. Aydil, *J. Appl. Phys.*, 2010, 108, 053303.
34. H. Yoshida, S. Takeda, T. Uchiyama, H. Kohno and Y. Homma, *Nano Lett.*, 2008, 8, 2082-2086.
35. M. Kumar and Y. Ando, *Journal of Nanoscience and Nanotechnology*, 2010, 10, 3739-3758.
36. B. D. Smith and R. R. White, *AIChE J.*, 1956, 2, 46-54.
37. X. Pan and X. Bao, *Chem. Commun.*, 2008, 6271-6281.
38. W. Chen, Z. Fan, X. Pan and X. Bao, *J. Am. Chem. Soc.*, 2008, 130, 9414-9419.
39. T. Herranz, S. Rojas, F. J. Pérez-Alonso, M. Ojeda, P. Terreros and J. L. G. Fierro, *J. Catal.*, 2006, 243, 199-211.
40. J. F. Shultz, W. K. Hall, B. Seligman and R. B. Anderson, *J. Am. Chem. Soc.*, 1955, 77, 213-221.
41. A. N. Pour, M. R. Housaindokht, S. F. Tayyari and J. Zarkesh, *J. Nat. Gas Chem.*, 2010, 19, 284-292.
42. R. M. Malek Abbaslou, J. Soltan and A. K. Dalai, *Fuel*, 2011, 90, 1139-1144.

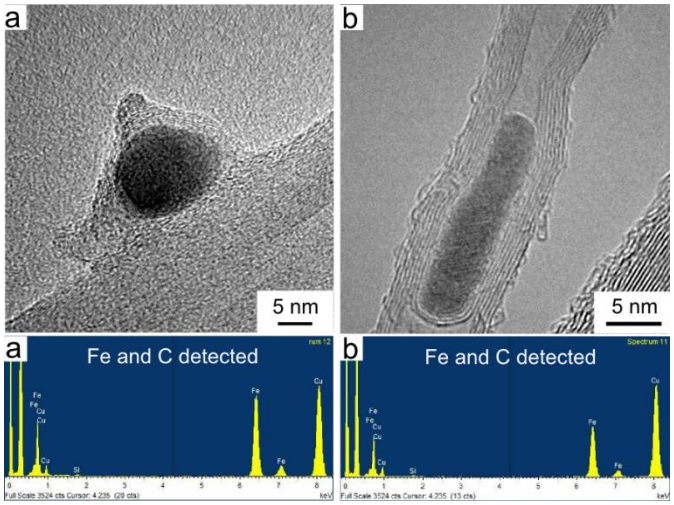

Figure S1 TEM micrographs of the two iron environments and elemental analysis a) outside of the tube, coated in a graphitic layer and b) inside the tube